Studies of Mn valence conversion and oxygen vacancies in $La_{1-x}Ca_xMnO_{3-y}$ using electron energy-loss spectroscopy

Z. L. Wang,[a] J. S. Yin, and Y. D. Jiang
School of Materials Science and Engineering, Georgia Institute of Technology, Atlanta, Georgia 30332-0245

Jiming Zhang[b]
Advanced Technology Materials, Inc., Danbury, Connecticut 06810

(Received 19 November 1996; accepted for publication 21 April 1997)

Using the white line intensities, electron energy-loss spectroscopy in a transmission electron microscope has been employed to characterize the valence conversion and oxygen vacancies in $La_{1-x}Ca_xMnO_{3-y}$. For a nominal doping composition $x=0.33$, the ratio of Mn^{4+} to Mn^{3+} is determined to be more than 0.25 but less than 0.5, and the content of oxygen vacancy y is no more than 0.065 (equivalent to 2.2 at. % of the oxygen content). At $y_{max}=0.065$, 60% of the residual charge introduced by Ca doping is balanced by the conversion of Mn^{3+} to Mn^{4+} and 40% by oxygen vacancy. © *1997 American Institute of Physics.* [S0003-6951(97)03725-X]

Colossal magnetoresistive (CMR) has been observed in a new class of oxides, (La,A)MnO_3(A=Ca, Sr, or Ba).[1–5] A very large magnetoresistance ratio ($\Delta R/R(H) > -100{,}000\%$) was reported in epitaxially grown $La_{0.67}Ca_{0.33}MnO_3$ films.[1] The new types of intrinsic magnetoresistive oxides offer exciting possibilities for improved magnetic sensors, magnetoresistive read heads, and magnetoresistive random access memory (MRAM). The potential for integration with silicon technology makes these oxides particularly attractive for applications in advanced technologies.[6]

The CMR magnetic oxides have a perovskite-type crystal structure with ferromagnetic ordering in the $a-b$ planes and antiferromagnetic ordering along the c axis. The ferromagnetically ordered Mn–O layers of the $a-b$ planes are isolated by a nonmagnetic La(A)–O monolayer. This spin-coupling structure is intrinsic. $La_{1-x}A_xMnO_3$ and $La_{1-x}A_xCoO_3$ compounds having the extreme values $x=0$, 1 are neither ferromagnetic nor good electrical conductors; they are semiconductors. Only compounds with intermediate values of x are ferromagnetic, with the strongest ferromagnetism occurring in the range $0.2<x<0.4$. Within this same range, the materials are electrically conductive for the following reason. The partial substitution of trivalent La^{3+} by divalent element A^{2+} is balanced by the conversion of Mn valence states between Mn^{3+} and Mn^{4+} (or Co^{3+} and Co^{4+} for Co) and the creation of oxygen vacancies as well. This valence state conversion of Mn was proposed by Jonker and van Santen,[7] and the ionic structure of $La_{1-x}A_xMnO_{3-y}$ is

$$La^{3+}_{1-x}A^{2+}_{x}Mn^{3+}_{1-x+2y}Mn^{4+}_{x-2y}O^{2-}_{3-y}V^{O}_{y}, \tag{1}$$

where V^{O}_{y} stands for the fraction of oxygen vacancies. Whenever a Mn^{3+} and a Mn^{4+} are on neighboring Mn sites, there exists the possibility of conductivity by electrons hopping from Mn^{3+} to $Mn^{4+}$with the assistance of the oxygen anion. That this hopping current should be spin polarized was required for a process of two simultaneous electron hops (from Mn^{3+} onto O^{2-} and from O^{2-} onto Mn^{4+}, thus interchanging Mn^{4+} and Mn^{3+}), called *double exchange*.[8] The electron hopping away from the Mn^{3+} remembers the spin state it has on the ion as determined by Hund's rule, and the electron hopping onto the Mn^{4+} must have the same spin state. This is only possible, without violating Hund's rule on the Mn^{4+}, if the net ion spins of the neighboring Mn^{3+} and Mn^{4+} are in the same spin direction. In fact, the likelihood of electron hopping between two magnetic ions turns out to depend on the spinor transformation,[9,10] which is characterized by a *transfer integral* (analogous to the transfer probability)

$$t_{ij}=b_{ij}\cos(\theta_{ij}/2), \tag{2}$$

where b_{ij} is a constant depending on the isolation between the ions, and θ_{ij} is the angle between the direction of the spin ions. Thus, the electric resistance of the material is a function of its intrinsic magnetic order. The angle between the spins of two ions will be changed under an external magnetic field. Thus, the electron transfer probability across the ions (or equivalently the conductivity) is affected according to Eq. (2), possibly leading to the observed CMR effect.

From Eq. (1), the local charge induced by the doping of A^{2+} is balanced by the conversion of Mn valence states from Mn^{3+} to Mn^{4+} and the creation of oxygen vacancies. As discussed following Eq. (2), the CMR effect may be entirely determined by the valence conversion between $Mn^{3+}$and Mn^{4+}. Thus, the creation of oxygen vacancies may reduce the double exchange effect, resulting in a decrease in the CMR ratio. In practice, however, quantifying of oxygen vacancies is a challenge to existing microscopy techniques although x-ray and neutron diffuse scattering can be used to determine vacancies in large bulk single crystalline specimens. Moreover, for thin films grown on a crystalline substrate the diffraction analysis may be strongly affected by the defects at the substrate-film interface and the surface disordering. In this letter, an alternative technique is introduced to determine the role played by oxygen vacancies in balancing the local charge in $La_{1-x}Ca_xMnO_{3-y}$ (LCMO).

$La_{1-x}Ca_xMnO_{3-y}$ (with a nominal composition $x=0.33$) films were grown on polished $LaAlO_3$(001) sub-

[a]Corresponding author. Electronic mail: zhong.wang@mse.gatech.edu
[b]Present address: Motorola, Inc., 3501 Ed Bluestein Blvd., MD: K-10 Austin, TX 78721.

 0003-6951/97/70(25)/3362/3/$10.00

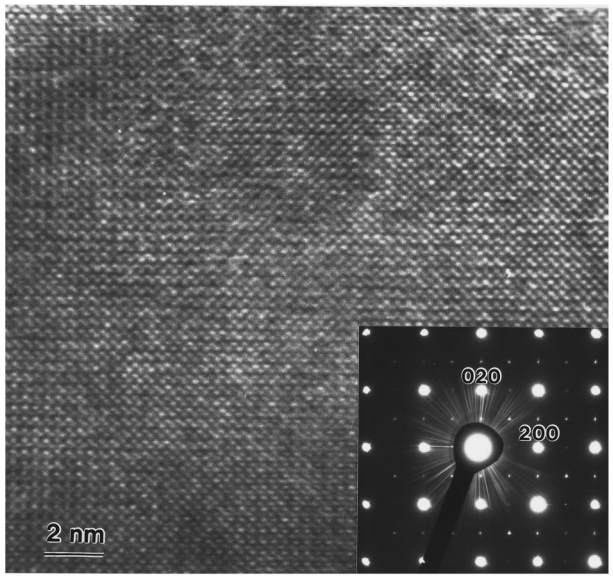

FIG. 1. [100] HRTEM image of LCMO and the corresponding electron diffraction pattern.

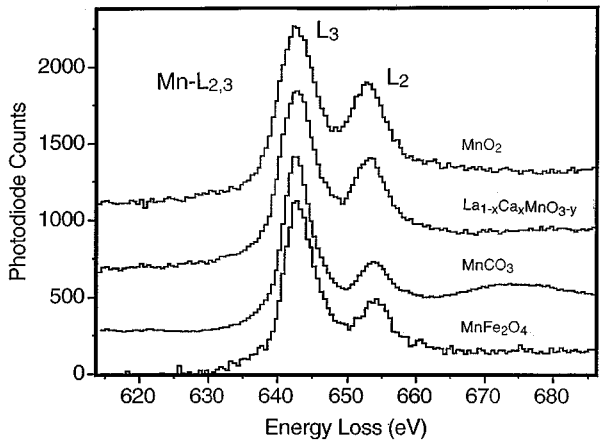

FIG. 2. Manganese $L_{2,3}$ edge spectra acquired from $Mn^{2+}Fe_2^{3+}O_4^{2-}$, $Mn^{2+}(CO_3)^{2-}$, $La_{1-x}^{3+}Ca_x^{2+}Mn_{1-x+2y}^{3+}Mn_{x-2y}^{4+}O_{3-y}^{2-}$, and $Mn^{4+}O_2^{2-}$, showing the dependence of the relative intensity of L_3 to L_2 on the valence state of Mn. The spectra were processed using the Fourier ratio method for removing the plural scattering effect (Ref. 13), and they are displayed after the subtraction of background. Each spectrum is shifted upward for comparison.

strates by liquid source metalorganic chemical vapor deposition (MOCVD) technique. Details of the liquid source MOCVD technique have been reported elsewhere.[5] High-resolution transmission electron microscopy (HRTEM) and electron energy-loss spectroscopy (EELS) experiments were performed at 200 kV using a Hitachi HF-2000 field emission gun TEM equipped with a Gatan 666 parallel-detection EELS.

Figure 1 shows an HRTEM image and an electron diffraction pattern recorded from the LCMO film. In contrast to the $La_{1-x}Sr_xCoO_3$ films reported previously,[11,12] no tetragonal domain structure is observed in the LCMO system. The grown film is single crystalline and no strong diffuse scattering features are observed in the electron diffraction pattern, indicating the ordering in lattice substitution of La by Ca and that the distribution of oxygen vacancies, if they exist, has no strong spatial correlation. From Eq. (1), the mean valence state of Mn is

$$\langle \mathrm{Mn} \rangle_{vs} = 3 + x - 2y, \tag{3}$$

where $x = 0.33$. The $\langle \mathrm{Mn} \rangle_{vs}$ can be determined using EELS as described below. Therefore, the content of oxygen vacancies y can be obtained.

For transition metals with unoccupied $3d$ and $4d$ states, white lines are observed in EELS.[13] The L_3 and L_2 lines are the transition of $2p^{3/2} \rightarrow 3d^{3/2}3d^{5/2}$ and $2p^{1/2} \rightarrow 3d^{3/2}$, respectively. The intensity ratio of the white lines $I(L_3)/I(L_2)$ has been shown by numerous experimental studies to depend sensitively and strongly on the valence state (or the occupation number of the d state) of the element.[14–23] This indicates that the valence state of the element can be determined experimentally using the white line intensity ratio in reference to the EELS spectra acquired from several standard specimens with known cation valence states. This is the principle of our analysis. Figure 2 gives a group of EELS spectra acquired from several compounds containing Mn with different valence states. The relative intensity of L_3 to L_2 changes dramatically as the valence state of Mn varies.[17,18] If the intensity is normalized at L_3, the intensity of L_2 for $MnFe_2O_4$ is the same as that of $MnCO_3$, while the L_2 line intensity for LCMO is higher than that of $MnFe_2O_4$ or $MnCO_3$ but smaller than that of MnO_2. This is the principle to be used for determining the mean valence state of Mn using EELS.

Figure 3 shows a plot of the experimentally measured intensity ratio of white lines $I(L_3)/I(L_2)$, calculated using the double-step background fitting procedure with the step at the peak.[19] This curve is nonlinear because the corrections

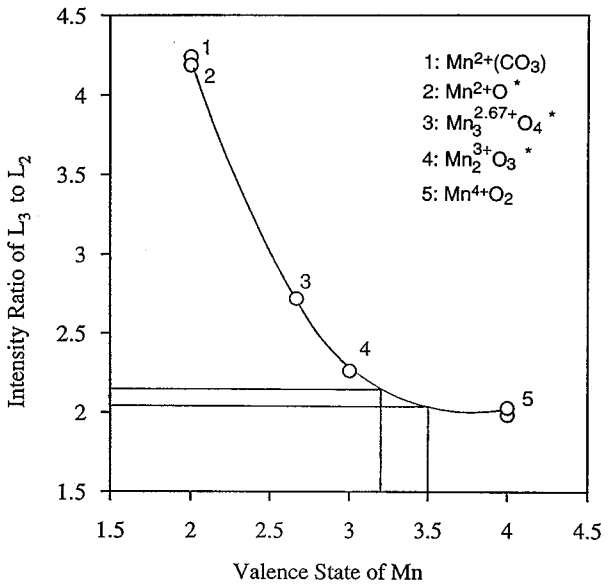

FIG. 3. A plot of white line intensity ratio $I(L_3)/I(L_2)$ vs the valence state of Mn for several standard specimens. A nominal fit of the experimental data is shown by a solid curve. The valence state of the LCMO film is obtained from the measured $I(L_3)/I(L_2)$ data, where a range including the experimental error is indicated, and the average valence state in LCMO is $\langle \mathrm{Mn} \rangle_{vs} = 3.2–3.5$. Asterisk (*) indicates the data adopted from Ref. 17 after applying the same background subtraction procedures. It must be pointed out that $I(L_3)/I(L_2)$ is a property of the inelastic excitation matrix elements and it is independent of the acceleration voltage of the electron microscope.

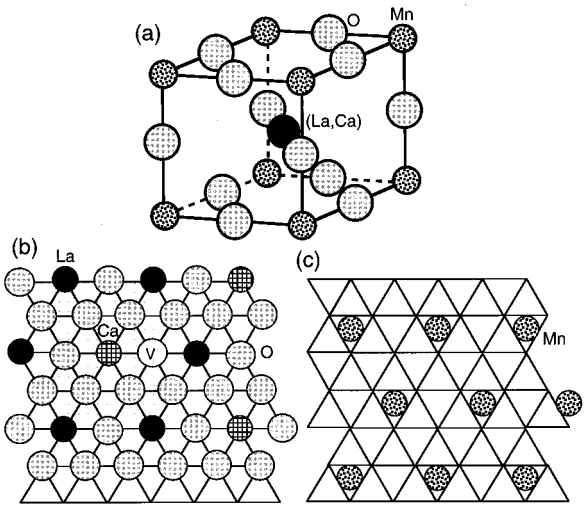

FIG. 4. (a) Three-dimensional unit cell of $La_{1-x}Ca_xMnO_3$ perovskite structure. (b) and (c) are the (111) (La,Ca)–O and the Mn close-packing layers, respectively, of the structure for $x=0.33$, where V indicates an oxygen vacancy.

made by the transition matrix elements of $R_{2p_{3/2}}$ and $R_{2p_{1/2}}$ for the L_3 and L_2 white lines, respectively, are not included in the calculation here.[19] On the other hand, if our analysis is based entirely on experimental data, this nonlinear curve can be applied equivalently to determine the valence state of Mn.[17,23] The $I(L_3)/I(L_2)$ ratio for LCMO is 2.05–2.17, thus, the average valence state of Mn is 3.2–3.5. Substituting this value into Eq. (3), yields $y \leqslant 0.065$, which is equivalent to less than 2.2 at. % of the oxygen content. At $y_{\max}=0.065$, the atom ratio of Mn^{4+} to Mn^{3+} in LCMO is 0.25, thus, the charge introduced by Mn valence conversion is $(x-2y)=0.2^+$, the charge due to oxygen vacancy is $2y=0.13^-$, which means that 60% of the residual charge introduced by Ca doping is balanced by the conversion of Mn^{3+} to Mn^{4+} and 40% by oxygen vacancies. This is a maximum estimation to the contribution made by oxygen vacancies. If the concentration of oxygen vacancy $y=0$, the atom ratio of Mn^{4+} to Mn^{3+} is 0.5. The relatively large uncertainty in the result is caused by the small difference between the $I(L_3)/I(L_2)$ values for Mn^{3-} and Mn^{4+}(see Fig. 3).

To qualitatively understand the creation of oxygen vacancies, an examination of the crystal structure of LCMO may be helpful. Figure 4(a) shows the unit cell of $(La,Ca)MnO_3$. If this structure is viewed parallel to the (111) plane, two fundamental stacking layers are introduced [Figs. 4(b) and 4(c)]. One type of layer is the close-packing of (La,Ca) and oxygen and the other layer is the packing of Mn alone. For $x=0.33$, the ratio of La to Ca is 2:1, thus, for an ordered structure, a Ca is likely to locate at the middle of six La atoms in the (111) plane. An oxygen vacancy, if it exists, is likely to be created adjacent to the Ca cation. Each oxygen vacancy is equivalent to supply $+2$ charge and the conversion of Mn^{3+} to Mn^{4+} gives a $+1$ charge; thus, the maximum concentration of oxygen vacancies required to balance the local charge is half of the doping amount at any circumstance, e.g., $y_{\max}=x/2$, which is $y_{\max}=0.165$ in our case. From the diffraction pattern shown in Fig. 1, the distribution of Ca in LCMO is likely to be ordered since the diffuse scattering generated by short-range order is not present in the diffraction pattern. On the other hand, no superstructure reflections are observed, indicating that the model proposed in Fig. 4(b) is likely to represent the Ca distribution in LCMO if the atom ratio Ca:La=1:2. For doping other than $x=0.33$, a superstructure due to the long-range order of Ca distribution is expected unless they are distributed randomly. The intensity ratio $I(L_3)/I(L_2)$ is almost independent of the specimen thickness and the deconvolution procedure and it is believed to be reliable for determination of valence states, as demonstrated by numerous examples.[21–23] Studies of $La_{0.5}Sr_{0.5}CoO_{2.25}$ crystal structure[24] and *in situ* reductions of Co_3O_4, MnO_2 and Fe_2O_3-Mn_2O_3 solid state solution[25] have also shown consistent results.

[1] K. Chahara, T. Ohno, M. Kasai, and Y. Kozono, Appl. Phys. Lett. **63**, 1990 (1993).
[2] R. von Helmolt, J. Wecker, B. Holzapfel, L. Schultz, and K. Samwer, Phys. Rev. Lett. **71**, 2331 (1994).
[3] S. Jin, T. H. Tiefel, M. McCormack, R. A. Fastnacht, R. Ramech, and L. H. Chen, Science **264**, 413 (1994).
[4] H. L. Ju, C. Kwon, R. L. Greenne, and T. Venkatessan, Appl. Phys. Lett. **65**, 2108 (1994).
[5] Y. Q. Li, J. Zhang, S. Pombrik, S. DiMascio, W. Stevens, Y. F. Yan, and N. P. Ong, J. Mater. Res. **10**, 2166 (1995); J. Zhang, R. A. Gardiner, P. S. Kirlin, R. W. Boerstler, and J. Steinbeck, Appl. Phys. Lett. **61**, 2884 (1992).
[6] G. A. Prinz, Physics Today, April, 58 (1995).
[7] G. H. Jonker and J. H. van Santen, Physica (Amsterdam) **19**, 120 (1953).
[8] C. Zener, Phys. Rev. **82**, 403 (1951).
[9] P. W. Anderson and H. Hasegawa, Phys. Rev. **100**, 675 (1955).
[10] P. G. de Gennes, Phys. Rev. **118**, 141 (1960).
[11] Z. L. Wang and J. Zhang, Philos. Mag. A **72**, 1513 (1995).
[12] Z. L. Wang and J. Zhang, Phys. Rev. B **54**, 1153 (1996).
[13] R. F. Egerton, *Electron Energy-loss Spectroscopy in the Transmission Electron Microscope*, 2nd ed. (Plenum, New York, 1996), p. 366.
[14] B. T. Thole and G. van der Laan, Phys. Rev. B **38**, 3158 (1988).
[15] D. M. Pease, S. D. Bader, M. B. Brodsky, J. I. Budnick, T. I. Morrison, and N. J. Zaluzec, Phys. Lett. A **114**, 491 (1986).
[16] T. I. Morrison, M. B. Brodsky, N. J. Zaluzec, and L. R. Sill, Phys. Rev. B **32**, 3107 (1985).
[17] H. Kurata and C. Colliex, Phys. Rev. B **48**, 2102 (1993).
[18] J. H. Rask, B. A. Mine, and P. R. Buseck, Ultramicroscopy **32**, 319 (1987).
[19] D. H. Pearson, C. C. Ahn, and B. Fultz, Phys. Rev. B **47**, 8471 (1993).
[20] D. H. Pearson, B. Fultz, and C. C. Ahn, Appl. Phys. Lett. **53**, 1405 (1988).
[21] J. L. Mansot, P. Leone, P. Euzen, and P. Palvadeau, Microsc. Microanal. Microstruct. **5**, 79 (1994).
[22] D. H. Person, C. C. Ahn, and B. Fultz, Phys. Rev. B **50**, 12969 (1994).
[23] J. A. Fortner and E. C. Buck, Appl. Phys. Lett. **68**, 3817 (1996).
[24] Z. L. Wang and J. S. Yin, Phil. Mag B (in press).
[25] Z. L. Wang, J. S. Yin, J. Z. Zhang, and W. D. Mo, J. Phys. Chem. (in press).